Research Article Vol. 29, No. 7 / 29 March 2021 / Optics Express 9711
Optics EXPRESS

Reconstruction of atomic resonances with attosecond streaking

ROCÍO BORREGO-VARILLAS[1] AND MATTEO LUCCHINI[1,2,*]

[1]Institute for Photonics and Nanotechnologies, IFN-CNR, 20133 Milano, Italy
[2]Department of Physics, Politecnico di Milano, 20133 Milano, Italy
[*]matteo.lucchini@polimi.it

Abstract: Recent development of spectroscopic techniques based on attosecond radiation has given the community the right tools to study the timing of the photoelectron process. In this work we investigate the effect of Fano resonances in attosecond streaking spectrograms and the application of standard phase-reconstruction algorithms. We show that while the existence of the infrared coupling (ac-Stark shift) hinders the applicability of FROG-like methods, under certain conditions it is still possible to use standard reconstruction algorithms to retrieve the photoemission delay of the bare resonance. Finally, we propose two strategies to study the strength of IR coupling using the attosecond streaking technique.

1. Introduction

The advent of attosecond science allowed the investigation of ultrafast electron dynamics with unprecedented time resolution, shedding new light onto very fundamental process [1,2]. Among all, the study of photoemission delays (attosecond chronoscopy [3]) has attracted considerable attention in the recent years [4–11]. In a typical experiment extreme-ultraviolet (XUV) attosecond radiation is used to ionize the target while an opportunely delayed and intense ($11^{11} - 11^{12}$ W/cm^2) infrared (IR) pulse probes the ionization mechanism by altering the final photoelectron energy. The collection of photoelectron spectra as a function of the XUV-IR delay is called RABBITT (reconstruction of attosecond beating by two-photon transitions) [12,13] or streaking trace [14,15] depending on the temporal characteristics of the XUV radiation: a train of attosecond pulses in the former case or an isolated attosecond pulse in the latter case. Both techniques are in principle capable of accessing photoemission delays [16] with some pros and cons on both sides. RABBITT is an interferometric technique which nicely combines time and frequency resolution [10] making it particularly suitable to study photoemisison delays in case of congested photoelectron spectra [17] as in molecules, liquids or solid samples [18–23]. Despite the great potentials of this technique [24], RABBITT samples the photoelectron phase with an energy step as wide as the separation between two consecutive harmonics (typically of about 3 eV), possibly preventing the reconstruction of the correct energy-dependent photoemission delay in case of quickly varying photoelectron phases, e.g. close to transition resonances [25,26]. Experiments based on the attosecond streaking techniques can in principle measure the energy-dependent photoelectron phase with higher energetic resolution, but its extraction from the experimental data is based on phase-retrieval procedures which often suffer of strong approximations [27].

Here we study how sharp atomic resonances affect the photoemission delays measured in attosecond streaking experiments [28]. In particular, proven that the attosecond streaking is sensitive to the photoemitted wavepacket even at the presence of phase jumps [29], we investigate whether this finding holds when an atomic resonance is dynamically modified by the IR field (namely, optical Stark shift). We show that while the existence of the IR coupling hinders the applicability of FROG-like methods, it is still possible to use standard reconstruction algorithms [30] to retrieve the photoemission delay of the bare atom. If on the one hand this justifies the application of FROG-CRAB reconstruction also in presence of a non negligible interaction with

#415463 https://doi.org/10.1364/OE.415463
Journal © 2021 Received 27 Nov 2020; revised 5 Mar 2021; accepted 5 Mar 2021; published 15 Mar 2021

Optics EXPRESS

the IR pulse, on the other hand this finding might suggest that attosecond streaking cannot be used to study the coupling with the field. We envision two possible ways to study the effect of IR coupling at the limit of relatively long or short IR pulses. If combined with more accurate reconstruction procedures [31–33] and precise experimental traces, our suggestion could lead to the investigation of the coupling between atomic resonances and an intense IR field with attosecond resolution.

2. Attosecond streaking in presence of a resonance

To investigate the role of atomic resonances in attosecond streaking experiments [14], we simulated streaking traces following the strong field approximation (SFA) [34] with the addition of the resonance term [35]. The total spectrogram, $S(\omega, \tau)$, can hence be written as the sum of two contributions (atomic units are used throughout the whole manuscript):

$$S(\omega, \tau) = |D(\omega, \tau) + R(\omega, \tau)|^2 , \tag{1}$$

where ω is the photoelectron kinetic energy, τ is the pump-probe delay, D and R represent the direct and resonant contribution, respectively. The direct part has the usual form:

$$D(\omega, \tau) = -i \int_{-\infty}^{+\infty} E_{XUV}(t_1 - \tau) d\left[\sqrt{2\omega} + A_{IR}(t_1)\right] e^{i\varphi(\omega, t_1)} e^{-i(I_p - \omega)t_1} dt_1, \tag{2}$$

where $d\left[\sqrt{2\omega}\right]$ is the dipole transition matrix element for the ground state to the continuum transition and the attosecond light pulse is presented by the electric field term $E_{XUV}(t_1)$. I_p is the atomic ionization potential and $\varphi(\omega, t_1)$ a phase term acquired by the electron during its motion in the continuum [36]:

$$\varphi(\omega, t_1) = \int_{t_1}^{+\infty} dt_3 \left[\sqrt{2\omega} A_{IR}(t_3) + \frac{A_{IR}(t_3)^2}{2}\right], \tag{3}$$

where, $A_{IR}(t)$ is the IR vector potential.

For a resonance characterized by a lifetime Γ, a complex parameter q, and a transition energy ω_{r0}, the resonant term can instead be written using the formalism proposed in [37]:

$$R(\omega, \tau) = -i \int_{-\infty}^{+\infty} \chi(t_1 - \tau) e^{i\varphi(\omega, t_1)} e^{-i(I_p - \omega)t_1} dt_1, \tag{4}$$

$$\chi(t_1 - \tau) = -i \frac{\Gamma}{2}(q - i) \int_{t_1}^{+\infty} E_{XUV}(t_2 - \tau) d\left[\sqrt{2\omega} + A_{IR}(t_2)\right] e^{\left(i\omega_{r0} - \frac{\Gamma}{2}\right)(t_2 - t_1)} dt_2, \tag{5}$$

As the effect of the transition dipole d has already been studied [29] and can be accounted for even in the reconstructions [33], in the following we will assume $d = 1$ in Eqs. (2) and 5. In this way we neglect the energy and IR dependence of the atomic dipole and focus on the resonance-field coupling effect. Within this approximation we can introduce a pulse function which represents the electron wavepacket (EWP) created by the XUV pulse at a delay τ:

$$P(t - \tau) = E_{XUV}(t - \tau) + \chi(t - \tau), \tag{6}$$

and a pure phase-gate function

$$G(t, \omega) = e^{i\varphi(\omega, t)}, \tag{7}$$

which allow Eq. (1) to be rewritten as:

$$S(\omega, \tau) = \left| -i \int_{-\infty}^{+\infty} dt P(t - \tau) G(t, \omega) e^{-i(I_p - \omega)t} \right|^2 . \tag{8}$$

Figure 1 shows the total spectrogram $S(\omega, \tau)$ and its direct and resonant components, $|D(\omega, \tau)|^2$ and $|R(\omega, \tau)|^2$, for an atomic resonance characterized by the following parameters: $\omega_{r0} = 150\,\text{eV}$,

Optics EXPRESS

$q = 2.2e^{i\pi/4}$, $\Gamma = 1/\tau_r$ and $\tau_r = 400$ as [28]. The photoemission is probed by a 200-as pulse centred at the 95$^{\text{th}}$ harmonic of the fundamental IR field ($\lambda_{IR} = 796$ nm), which lies about 2 eV below the resonance. The IR field lasts for 2.5 optical cycles and has a peak intensity of $I_{IR} = 2 \times 10^{12}$ W/cm^2. Even if the resonance lifetime is relatively small (400 as), the resonant contribution shows a clear tail (red curve in Fig. 1(a)), which strongly modifies the overall temporal profile of $P(t)$. In the frequency domain this translates into the appearance of a peak at $\omega = \omega_{r0}$ (Fig. 1(b)) to which is associated a strong phase variation (Fig. 1(c)). Since the total electron burst $P(t)$ lasts for more than an IR optical cycle, $T_c = 2.665$ fs, $|R(\omega,\tau)|^2$ and $S(\omega,\tau)$ show characteristic fringes which are not present in $|D(\omega,\tau)|^2$ and could be used to determine the properties of the atomic resonance [28,29].

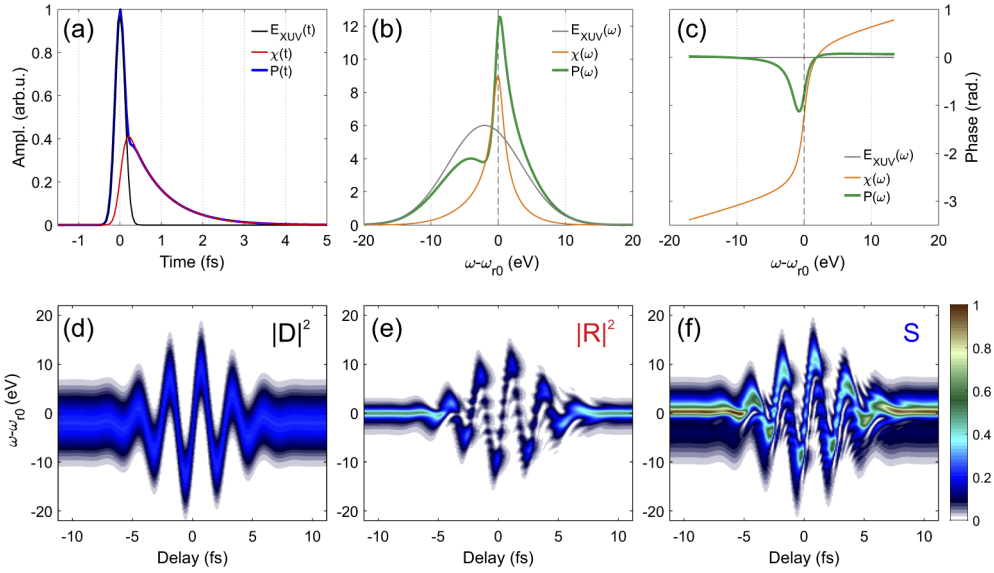

Fig. 1. **(a)** Temporal behaviour of electron wavepacket $P(t)$ (blue curve) an its direct and resonant components: $E_{XUV}(t)$ and $\chi(t)$ (black and red curves, respectively). Spectral amplitude, **(b)**, and phase, **(c)**, of the quantities reported in (a). Calculated spectrograms $|D(\omega,\tau)|^2$, **(d)**, $|R(\omega,\tau)|^2$, **(e)** and $S(\omega,\tau)$, **(f)**. Calculations parameters: XUV full-width-half-maximum (FWHM) = 200 as, XUV center energy 147.97 eV (corresponding to the 95$^{\text{th}}$ harmonic), IR FWHM = $2.5T_c$ where $T_c = 2.665$ fs is the optical cycle. IR intensity $I_{IR} = 2 \times 10^{12}$ W/cm^2, $\omega_{r0} = 150$ eV, $q = 2.2e^{i\pi/4}$, $\Gamma = 1/\tau_r$ and $\tau_r = 400$ as.

Here we are interested in the particular case where the resonance is coupled to the IR electric field $E_{IR}(t)$. For the sake of simplicity, let us consider the situation in which E_{IR} modifies the bare resonance energy ω_{r0} through optical Stark effect [38] as follows:

$$\omega_r(t) = \omega_{r0} - \alpha E_{IR}(t)^2, \tag{9}$$

with α being a polarizability factor characteristic of the target under examination. In an attosecond streaking experiment the temporal waveform of the IR electric field is actively stabilized, assuring $E_{IR}(t)$ to repeat itself unaltered at each laser pulse. Through ionization, the attosecond pulse is thus capable to resolve not only the IR pulse envelope, but also the actual amplitude oscillations of the electric field. For this reason, in Eq. (9) we consider the instantaneous value of $E_{IR}(t)$ instead of its cycle average, as done in majority of the cases when treating the optical Stark effect. By substituting $\omega_r(t)$ to ω_{r0} in Eq. (5) one immediately notices that a non-zero α induces a complex delay dependence in χ, the resonant contribution to the electron wavepacket. The first

Optics EXPRESS

raw in Fig. 2 shows four spectrograms calculated with the same parameters as in Fig. 1, but with an increasing value of α. While a clear distortion of the spectrogram is visible only for strong couplings (Figs. 2(c), (d)), already at smaller values of α both the spectral amplitude (second row in Fig. 2) and phase of the EWP are no longer constant, but change with the pump-probe delay τ, presenting a complex oscillation pattern which follows the square of the IR electric field. The effect becomes clear when studying the phase delay acquired by the EWP at each τ during the photoemission process, reported in the third row in Fig. 2 and defined as [39]:

$$\theta_\alpha(\omega,\tau) = \frac{\partial \arg\left[P(\omega,\tau)\right]}{\partial\omega}, \tag{10}$$

where $\arg[P]$ indicates the phase of the EWP in frequency domain. θ_α displays variations as big as several tens of attoseconds, which should be detectable with the accuracy of the current experimental techniques [40]. Nevertheless, since the EWP $P(t)$ does not shift rigidly with the delay τ, but changes its shape and phase at each delay point, the factorization reported in Eq. (8) is no longer possible, hindering, in principle, the correct applicability of FROG-based phase reconstruction algorithms when $\alpha \neq 0$.

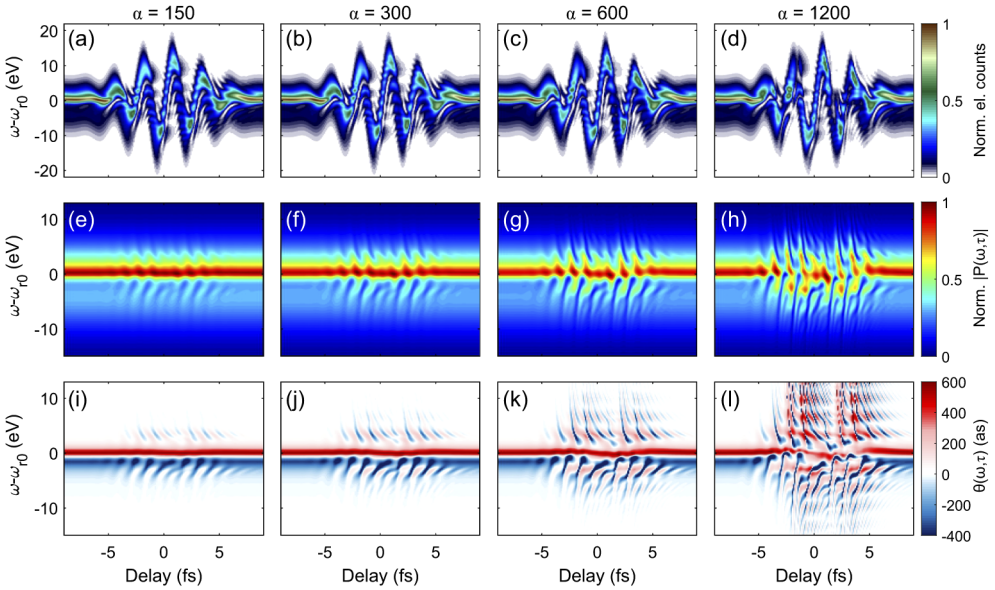

Fig. 2. **(a)-(d)**, Simulated streaking traces with a polarizability factor α of 150, 300, 600 and 1200, respectively. **(e)-(h)**, Normalized modulus of the electron wavepacket Fourier transform $P(\omega,\tau)$, for increasing value of α as in the upper row. **(i)-(l)**, Associated phase delay $\theta(\omega,\tau)$. In all the simulations the pulses and resonance parameters are the same as in Fig. 1.

3. Photoemission delays close to Fano resonances

Despite what found in the previous section, as the IR-induced changes onto the EWP oscillate along the pump-probe delay axis, one could think to apply FROG-like reconstruction algorithms nevertheless and retrieve an average $P(t)$. In this section we investigate this possibility and apply standard reconstruction algorithms to streaking traces characterized by resonance transitions. At first we concentrate on the case with no (or negligible) coupling to the IR field to prove that the algorithm works within its applicability domain. Later we address the case of $\alpha \neq 0$.

Optics EXPRESS

3.1. No IR coupling: $\alpha = 0$

One common approach to retrieve the phase of the EWP from the spectrogram $S(\omega, \tau)$ consists in employing the FROG-CRAB formalism [7,15,16]. By subsisting ω with the central photon energy ω_c in Eq. (7) (so called central momentum approximation, CMA), one can remove the energy dependence in $G(t, \omega)$. The product of Eq. (8) becomes then an internal product and the spectrogram can be treated with FROG-based phase retrieval algorithms like the extended ptychographic iterative engine (ePIE) [30]. Figure 3(a) shows the reconstructed spectrogram after 15000 iterations of the ePIE algorithm for the simulated streaking trace of Fig. 1(f) where no coupling between the resonance and the IR field has been considered ($\alpha = 0$). In this particular case $P(t)$ shifts rigidly with the value of the delay τ and it can be fairly well reconstructed (Fig. 3(b)) despite of the CMA. The same holds for the IR vector potential, $A_{IR}(t)$ (Fig. 3(c)), and the spectral amplitude and phase of P (Fig. 3(d) and Fig. 3(e)). Since the photoemission delay $\theta_0(\omega)$ does not depend on τ, it can be nicely reconstructed (Fig. 3(f)). This result proves that ePIE can be applied to retrieve small photoemission delays if the optical Stark effect is negligible and if the CMA and wave-packet approximations are legitimate. The situation may change when $\alpha \neq 0$ as discussed in the next subsection.

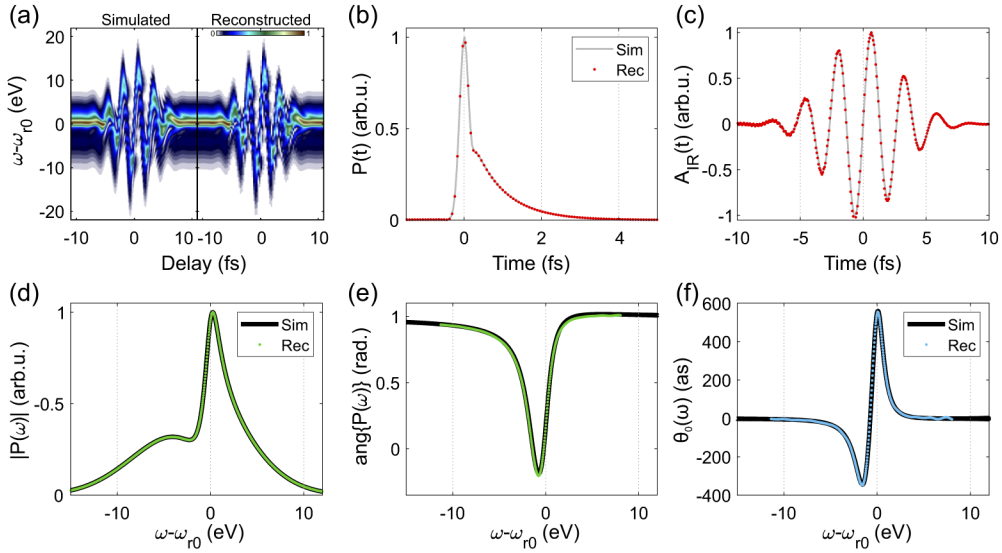

Fig. 3. **(a)** Simulated and ePIE-reconstructed streaking trace for the straking trace reported in Fig. 1 (f) where there is no coupling between the IR field and the resonance ($\alpha = 0$). Simulated (solid line) and reconstructed (red dots) temporal profiles of the attosecond electron burst $P(t)$, **(b)**, and the IR vector potential, **(c)**. Fourier transforming $P(t)$ results in the spectral amplitude and phase reported in **(e)** and **(d)**, respectively. **(f)**, Comparison between the simulated and reconstructed phase delay defined by Eq. (10).

3.2. Influence of the IR coupling: $\alpha \neq 0$

As discussed in Sec. 2., when $\alpha \neq 0$ the EWP P changes with the pump-probe delay τ, and therefore it is not possible to predict the relation between the ePIE reconstruction output and the actual EWP. Nevertheless, since ePIE considers all the delay points, we may expect the reconstruction results to agree with the delay-averaged $P(\omega, \tau)$. Indeed, since the modifications induced by the IR field over the electron burst oscillate with τ (see Fig. 2, third row), one can expect that the effect will average and vanish for sufficiently long IR pulses. To study this we computed the total photoelectron spectrogram assuming the same parameters as in Fig. 3, but

Optics EXPRESS

changing the IR time duration and the value of α. The resulting traces have been reconstructed with ePIE under the same conditions as in the case $\alpha = 0$. Figure 4 shows a comparison between the simulated (solid gray) and the ePIE-reconstructed (colored curves) phase delay θ and $A_{IR}(t)$ for different values of α and for four IR pulse durations. At this IR intensity, we found the reconstruction result to agree with the naked resonance ($\alpha = 0$) for relatively small values of α (smaller than 600), independently from the IR pulse duration. For strong coupling with the field, both the properties of the reconstructed EWP and IR are modified with the strongest reconstruction error being on the IR. This is a property already observed for the ePIE algorithm [41], which is more robust in the reconstruction of $P(t)$ and tends to project the reconstruction error on $G(t)$, *i.e.* on the IR vector potential. Furthermore we notice that, the effect of a non-zero field coupling over the reconstruction is stronger for longer IR pulses. At the limit of IR pulses with a duration of half optical cycle (Figs. 4(d) and 4(f)) the reconstructed IR field and EWP phase agree nicely with the bare case even for values of α as big as 1200. This seems to be unexpected as for short IR pulses the ePIE algorithm does not have enough significant delay points to perform an average and should therefore produce a stronger deviation from the case with $\alpha = 0$. Nevertheless, short IR pulses produce a weaker modification of the EWP properties (compare top and bottom rows in Fig. 5), thus explaining the better agreement for short pulse lengths.

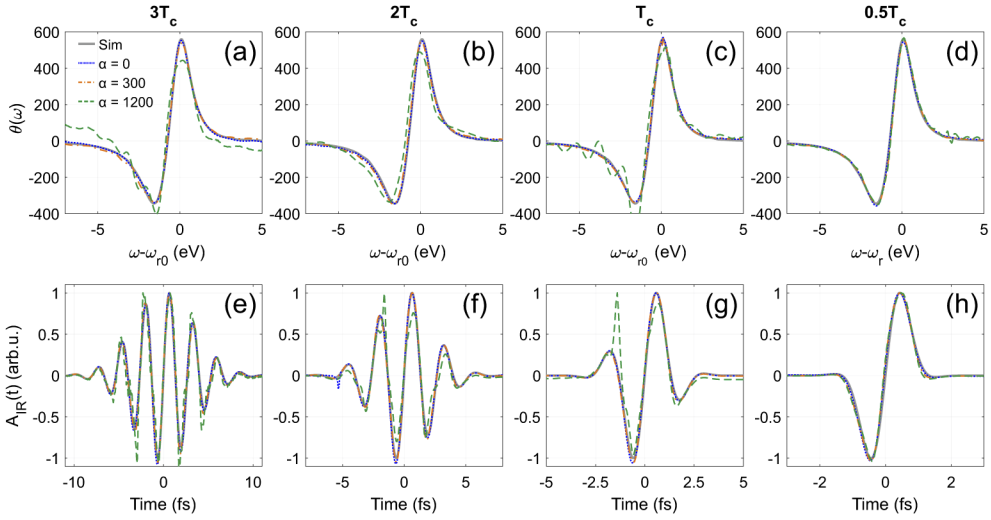

Fig. 4. **(a)** Comparison between the simulated (solid gray) and reconstructed (colored curves) phase delay extracted from a spectrogram generated with IR pulses with a duration of 3 times the optical cycle T_c and a coupling factor α equal 0 (dotted blue), 300 (dash-dotted orange) and 1200 (dashed green). **(b)-(d)**, Same as in (a) but with and IR pulse duration of 2, 1 and 0.5 T_c, respectively. **(e)** Simulated (solid grey) and reconstructed (broken curves) IR vector potential referring to the simulations in (a). **(f)-(h)**, Same as (e) but pertaining to the reconstructions in (b), (c) and (d), respectively.

On the one hand, these results show that ePIE can still be used to reconstruct the bare photoemission delay, $\theta_0(\omega)$, even if the EWP is no longer constant along the spectrogram. On the other hand, the fact that ePIE reconstructs the same EWP and IR pulse independently from the value of α means that this approach is not sensitive to the IR laser coupling and cannot be used, as it is, to study this effect. In the next sections we propose two different ways to overcome this limit when employing short or long IR pulses.

Optics EXPRESS

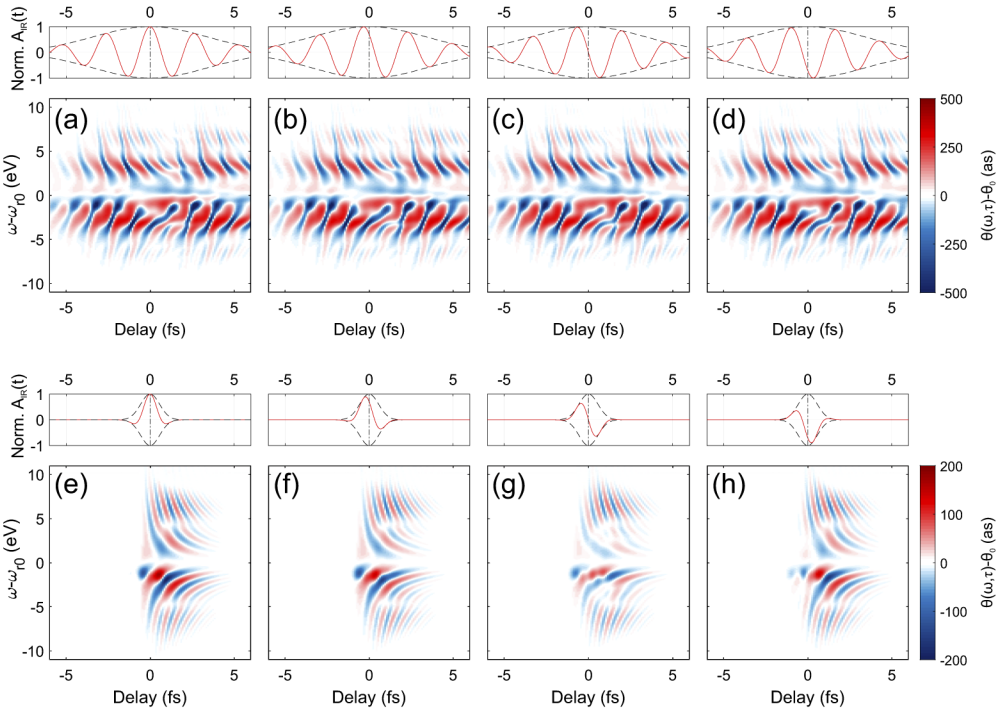

Fig. 5. **(a)**-**(d)**, Induced variation in the phase delay defined as $\theta_\alpha(\omega,\tau) - \theta_0$, for an IR vector potential with FWHM of $3T_c$ and CEP, ϕ_0 of 0, $\pi/4$, $\pi/2$ and $3\pi/4$, respectively. The upper panels show the associated normalized $A_{IR}(t)$. **(e)**-**(h)**, Same quantities but for an IR FWHM of $0.5T_c$. In all cases $\alpha = 300$. The other simulations parameters are the same as in Fig. 1.

4. Short pulse limit: CEP dependence

As discussed in the previous sections the ac-Stark shift of the resonance causes a rich oscillation pattern in the photoemission delay $\theta_\alpha(\omega,\tau)$ (Fig. 2). Even if locally the differences with the bare photoemission delay $\theta_0(\omega)$ can be of several tens to hundreds of as, due to the oscillations the effect is strongly reduced when considering the delay average over the full scan. With short IR pulses, however, the length of the streaking trace might contain a reduced number of oscillations and the delay average of $\theta_\alpha(\omega,\tau)$ might substantially differ from $\theta_0(\omega)$. In addition, the exact pattern of $\theta_\alpha(\omega,\tau)$ may also depend on the IR field carrier-envelope phase (CEP). As the exact magnitude of the CEP dependence changes with the values of α, this might suggest a new way of extracting information about the resonance-field coupling. The methodology could be the following: *i*) perform a streaking experiment with a given value of the IR CEP and retrieve the associated EWP energy-dependent photoemission delay; *ii*) change the value of the IR CEP and repeat the measurement, *iii*) compare the photoemission delays. The magnitude of the IR coupling can then be retrieved by comparing the experimental results with the theoretical prediction.Fig. 5 shows the IR-induced changes to the EWP by reporting the differences between the calculated photoemission delay with $\alpha = 300$, $\theta_\alpha(\omega,\tau)$, and the photoemission delay of the bare resonance, $\theta_0(\omega)$ (obtained with $\alpha = 0$). The top row presents the calculations for an IR pulse duration of $3\,T_c$, while the bottom row is obtained for an IR duration of $0.5\,T_c$. The different columns are associated with a different value of the IR CEP as displayed at the top panel. Under the same coupling conditions, longer IR pulses induce a stronger modification on the photoemission delay θ_α while with short pulses there is a clearer effect of the IR CEP.

Optics EXPRESS

Moreover, for sufficiently short IR pulses, the CEP dependence persists also when the full trace is considered. Figure 6 shows the delay-averaged IR induced changes in the photoemission delay $\langle\theta(\omega_\alpha,\tau)-\theta_0\rangle$ calculated for different CEPs and time durations of the IR pulse with $\alpha = 300$. As it is possible to notice, a clear CEP dependence appears when the IR pulse duration is comparable to one optical cycle. While this may open the possibility to investigate such an effect with attosecond streaking and FROG-like algorithms, an increasing CEP dependence comes together with a smaller maximum value of $\langle\theta(\omega_\alpha,\tau)-\theta_0\rangle$ (less than 1 as in Fig. 6(d)). Detecting a CEP dependence in the delay-averaged photoemission delay becomes therefore quite challenging as it calls for extremely short IR pulses and the need of refined reconstruction algorithms, which are not based on the CMA or the wave-packet approximation [32,33,42], to guarantee higher temporal resolution.

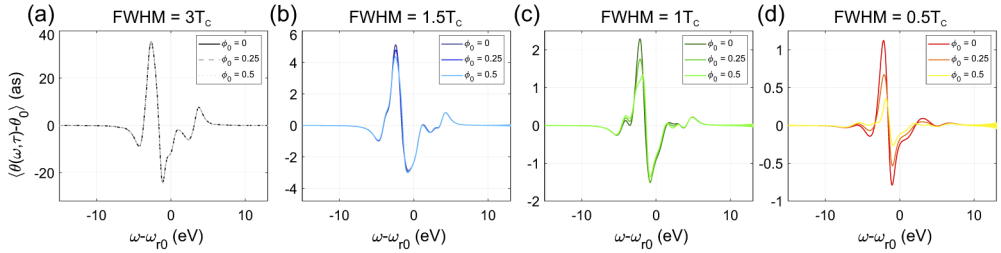

Fig. 6. **(a)** Difference between the delay-averaged phase delay of the electron wavepacket $\langle\theta_\alpha(\omega,\tau)\rangle$ and the naked resonance phase delay $\theta_0(\omega)$, for a coupling parameter $\alpha = 300$, an IR FWHM of $3T_c$ and three different values of the IR vector potential CEP ϕ_0. **(b)**-**(d)**, Same quantities but for an IR FWHM of $1.5T_c$, T_c and $0.5T_c$, respectively. All the other simulation parameters are kept the same as in Fig. 1.

5. Long pulse limit: cycle-averaged phase

A different approach, which relaxes at least the experimental difficulties, could be based on the employment of a longer IR pulse. Indeed with relatively long IR pulses one can obtain instantaneous modifications of the photoemission delay as big as 500 as (Figs. 5(a)-(d)), which remain visible also if the photoemission delay is averaged over an optical cycle.

The plot in Fig. 7(a) reports the photoemission delays of Fig. 5(c) averaged over T_c, $\langle\theta_\alpha(\omega,\tau)-\theta_0\rangle_{T_c}$. Figure 7(b) shows $\langle\theta_\alpha(\omega,\tau)-\theta_0\rangle_{T_c}$ at four chosen values of τ, corresponding to the portions of streaking trace highlighted in Fig. 7(c). Clear variations, as big as 180 as can be observed even without subtracting the photoemission delay of the bare resonance (Fig. 7(d)). Since the reconstruction algorithms need only a portion of trace as wide as one IR optical cycle to obtain a reliable reconstruction of the EWP, one can study the effect of the resonance-field coupling by slicing the streaking spectrogram in portions as wide as T_c and reconstructing them individually. In this approach, the first portion at relatively big pump-probe delays can be used to estimated the naked resonance while the portions of spectrogram around $\tau = 0$ fs can be used to evaluate the effect of the IR field. Unfortunately, we found CMA-based algorithms (ePIE [30,41], the principal component generalized projection algorithm, PCGPA [43] and the least square generalized projection algorithm, LSGPA [44]) to fail in reconstructing the phase delays of Fig. 7(d). We observe the main limitation to be artifacts introduced by the limited delay window of the spectrogram portions used in the reconstruction. The problem can therefore be solved by using different algorithms capable of run over partial spectrograms [42]. A detailed study of the applicability of such algorithms goes beyond the scope of the present work.

It is worth noticing that an approach based on the slicing of the streaking trace will not work for short IR pulses. Figure 8 shows the same quantities as in Fig. 7, simulated under the same

Optics EXPRESS

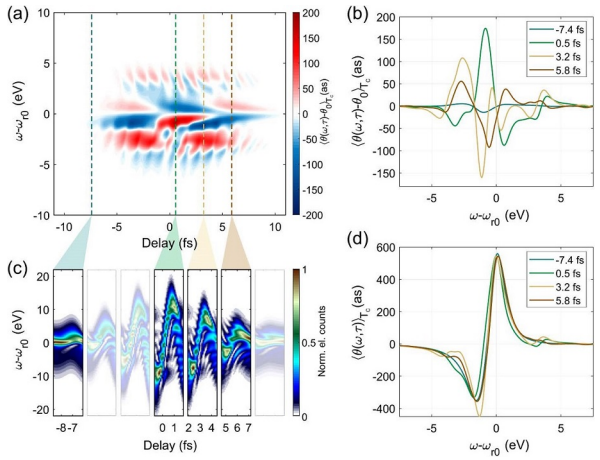

Fig. 7. **(a)** Cycle-averaged phase delay difference, $\langle\theta_\alpha(\omega,\tau)-\theta_0\rangle_{T_c}$, for an IR FWHM of $3T_c$, CEP of $\pi/2$ and coupling parameter $\alpha = 300$. **(b)** Layouts from (a) at four different pump-probe delays. **(c)**, Portions of the initial streaking trace of length equal to one optical cycle T_c, centered at the selected pump-probe delays in (a). **(d)**, Associated cycle-averaged phase delay, $\langle\theta_\alpha(\omega,\tau)\rangle_{T_c}$.

conditions, but for an IR pulse duration of $0.5\,T_c$. As it is possible to observe, the IR effect is reduced by an order of magnitude, giving almost identical photoemission delays for every portion selected (Fig. 8(d)).

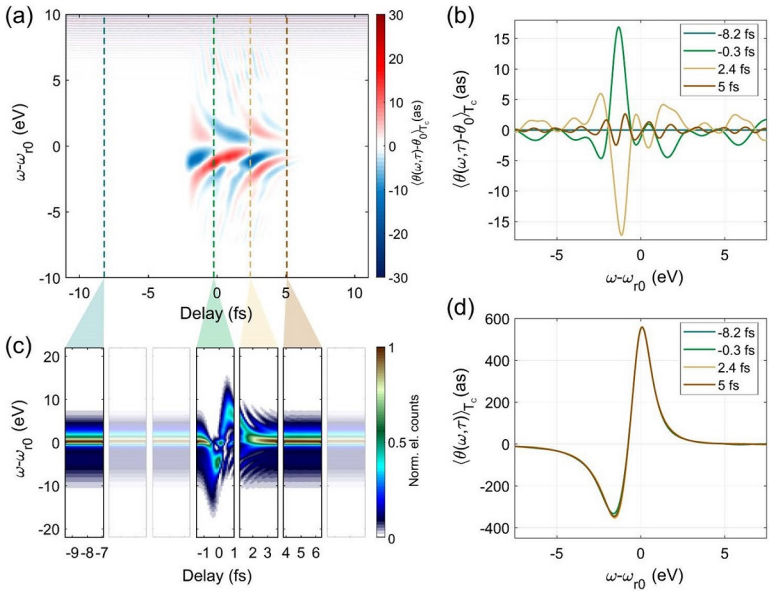

Fig. 8. **(a)** Cycle-averaged phase delay difference, $\langle\theta_\alpha(\omega,\tau)-\theta_0\rangle_{T_c}$, for an IR FWHM of $0.5T_c$, CEP of $\pi/2$ and coupling parameter $\alpha = 300$. **(b)** Layouts from (a) at four different pump-probe delays. **(c)**, Portions of the initial streaking trace of length equal to one optical cycle T_c, centered at the selected pump-probe delays in (a) and (b). **(d)**, Associated cycle-averaged phase delay, $\langle\theta_\alpha(\omega,\tau)\rangle_{T_c}$.

Optics EXPRESS

6. Conclusions

We investigated the role of atomic resonances in attosecond streaking spectrograms and the application of phase-reconstruction algorithms to retrieve information on the photoemission delay and the coupling of an IR pulse with a resonance. We found that in case of no coupling with the IR field, the spectrogram can be factorized as an internal product, allowing the application of phase-reconstruction algorithms. When a non-zero coupling with the field exists, this factorization is no longer possible and there is no a-priori knowledge on the physical meaning of the reconstructed quantities. If the algorithm employed is ePIE, our results show that the reconstructed photoemission delay corresponds to the expected frequency derivative of the bare EWP spectral phase (i.e. no IR coupling) within the reconstruction accuracy. Appreciable reconstruction artifacts are observed only for relatively big coupling with the IR field and to the long IR pulse limit. On the one hand, this finding justifies the application of reconstruction algorithms to extract the bare photoemission delay even if a weak IR coupling is present. On the other hand, it seems to preclude the possibility to use standard attosecond streaking experiments to study the coupling between the IR pulse and the atomic resonances. We propose two different ways overcome this limit and study the IR coupling with attosecond streaking. Our simulations reveal that in the short pulse limit, the average photoemission delay encoded in the spectrogram becomes CEP dependent. The stronger the coupling, the stronger the variations induced with the CEP. The availability of a more accurate reconstruction scheme could then open the possibility to investigate the coupling strength by comparing the reconstruction of traces recorded with IR pulses characterized by a different CEP. Moving to the opposite limit (long IR pulses), one can instead compare the photoemission delays obtained by reconstructing portions of the same spectrogram as wide as one optical cycle. Our results indicate that in this regime the cycle-average phase of the EWP presents variations as big as several tens of attoseconds, whose exact amplitude depends on the coupling between the resonance and the IR pulse. While the actual FROG-CRAB reconstruction schemes should be able to reconstruct the EWP phase starting from portions of the full streaking trace, we found that the accuracy of the reconstruction is strongly reduced when the algorithms are applied to partial traces, preventing the retrieval of the phase differences induced by the resonance-IR coupling. We expect our findings to stimulate the development of more accurate reconstruction techniques which, in tandem with precise experimental measurements, will allow for shedding new light onto ultrafast electron dynamics underling the photoemission process.

Funding. Ministero dell'Istruzione, dell'Università e della Ricerca (MIUR) under the PRIN programme (2017RKWTMY, aSTAR); European Research Council under the European Union's Horizon 2020 research and innovation programme (848411, AuDACE).

Acknowledgments. The authors wish to thank Luca Argenti for the fruitful scientific discussion.

Disclosures. The authors declare no conflicts of interest.

Data availability. Data underlying the results presented in this paper are not publicly available at this time but may be obtained from the authors upon reasonable request.

References

1. F. Krausz and M. Ivanov, "Attosecond physics," Rev. Mod. Phys. **81**(1), 163–234 (2009).
2. M. Nisoli, P. Decleva, F. Calegari, A. Palacios, and F. Martin, "Attosecond electron dynamics in molecules," Chem. Rev. **117**(16), 10760–10825 (2017).
3. R. Pazourek, S. Nagele, and J. Burgdörfer, "Attosecond chronoscopy of photoemission," Rev. Mod. Phys. **87**(3), 765–802 (2015).
4. A. L. Cavalieri, N. Müller, T. Uphues, V. S. Yakovlev, A. Baltuška, B. Horvath, B. Schmidt, L. Blümel, R. Holzwarth, S. Hendel, M. Drescher, U. Kleineberg, P. M. Echenique, R. Kienberger, F. Krausz, and U. Heinzmann, "Attosecond spectroscopy in condensed matter," Nature **449**(7165), 1029–1032 (2007).
5. M. Schultze, M. Fiess, N. Karpowicz, J. Gagnon, M. Korbman, M. Hofstetter, S. Neppl, A. L. Cavalieri, Y. Komninos, T. Mercouris, C. A. Nicolaides, R. Pazourek, S. Nagele, J. Feist, J. Burgdorfer, A. M. Azzeer, R. Ernstorfer, R.

Optics EXPRESS

Kienberger, U. Kleineberg, E. Goulielmakis, F. Krausz, and V. S. Yakovlev, "Delay in Photoemission," Science **328**(5986), 1658–1662 (2010).
6. K. Klünder, J. M. Dahlström, M. Gisselbrecht, T. Fordell, M. Swoboda, D. Guénot, P. Johnsson, J. Caillat, J. Mauritsson, A. Maquet, R. Taïeb, and A. L'Huillier, "Probing Single-Photon Ionization on the Attosecond Time Scale," Phys. Rev. Lett. **106**(14), 143002 (2011).
7. M. Sabbar, S. Heuser, R. Boge, M. Lucchini, T. Carette, E. Lindroth, L. Gallmann, C. Cirelli, and U. Keller, "Resonance effects in photoemission time delays," Phys. Rev. Lett. **115**(13), 133001 (2015).
8. L. Cattaneo, J. Vos, R. Y. Bello, A. Palacios, S. Heuser, L. Pedrelli, M. Lucchini, C. Cirelli, F. Martín, and U. Keller, "Attosecond coupled electron and nuclear dynamics in dissociative ionization of H_2," Nat. Phys. **14**(7), 733–738 (2018).
9. J. Vos, L. Cattaneo, S. Patchkovskii, T. Zimmermann, C. Cirelli, M. Lucchini, A. Kheifets, A. S. Landsman, and U. Keller, "Orientation-dependent stereo Wigner time delay and electron localization in a small molecule," Science **360**(6395), 1326–1330 (2018).
10. M. Isinger, R. J. Squibb, D. Busto, S. Zhong, A. Harth, D. Kroon, S. Nandi, C. L. Arnold, M. Miranda, J. M. Dahlström, E. Lindroth, R. Feifel, M. Gisselbrecht, and A. L'Huillier, "Photoionization in the time and frequency domain," Science **358**(6365), 893–896 (2017).
11. S. Biswas, B. Förg, L. Ortmann, J. Schötz, W. Schweinberger, T. Zimmermann, L. Pi, D. Baykusheva, H. A. Masood, I. Liontos, A. M. Kamal, N. G. Kling, A. F. Alharbi, M. Alharbi, A. M. Azzeer, G. Hartmann, H. J. Wörner, A. S. Landsman, and M. F. Kling, "Probing molecular environment through photoemission delays," Nat. Phys. **16**(7), 778–783 (2020).
12. H. G. Muller, "Reconstruction of attosecond harmonic beating by interference of two-photon transitions," Appl. Phys. B: Lasers Opt. **74**(S1), s17–s21 (2002).
13. P. M. Paul, "Observation of a Train of Attosecond Pulses from High Harmonic Generation," Science **292**(5522), 1689–1692 (2001).
14. J. Itatani, F. Quéré, G. L. Yudin, M. Y. Ivanov, F. Krausz, and P. B. Corkum, "Attosecond streak camera," Phys. Rev. Lett. **88**(17), 173903 (2002).
15. Y. Mairesse and F. Quéré, "Frequency-resolved optical gating for complete reconstruction of attosecond bursts," Phys. Rev. A **71**(1), 011401 (2005).
16. L. Cattaneo, J. Vos, M. Lucchini, L. Gallmann, C. Cirelli, and U. Keller, "Comparison of attosecond streaking and rabbitt," Opt. Express **24**(25), 29060–29076 (2016).
17. I. Jordan and H. J. Wörner, "Extracting attosecond delays from spectrally overlapping interferograms," J. Opt. **20**(2), 024013 (2018).
18. M. Huppert, I. Jordan, D. Baykusheva, A. von Conta, and H. J. Wörner, "Attosecond Delays in Molecular Photoionization," Phys. Rev. Lett. **117**(9), 093001 (2016).
19. J. Caillat, A. Maquet, S. Haessler, B. Fabre, T. Ruchon, P. Salières, Y. Mairesse, and R. Taïeb, "Attosecond Resolved Electron Release in Two-Color Near-Threshold Photoionization of N_2," Phys. Rev. Lett. **106**(9), 093002 (2011).
20. I. Jordan, M. Huppert, D. Rattenbacher, M. Peper, D. Jelovina, C. Perry, A. V. Conta, A. Schild, H. J. Wörner, and M. Carlo, "Attosecond spectroscopy of liquid water," Science **369**(6506), 974–979 (2020).
21. M. Lucchini, L. Castiglioni, L. Kasmi, P. Kliuiev, A. Ludwig, M. Greif, J. Osterwalder, M. Hengsberger, L. Gallmann, and U. Keller, "Light-Matter Interaction at Surfaces in the Spatiotemporal Limit of Macroscopic Models," Phys. Rev. Lett. **115**(13), 137401 (2015).
22. L. Kasmi, M. Lucchini, L. Castiglioni, P. Kliuiev, J. Osterwalder, M. Hengsberger, L. Gallmann, P. Krüger, and U. Keller, "Effective mass effect in attosecond electron transport," Optica **4**(12), 1492 (2017).
23. Z. Tao, C. Chen, T. Szilvási, M. Keller, M. Mavrikakis, H. Kapteyn, and M. Murnane, "Direct time-domain observation of attosecond final-state lifetimes in photoemission from solids," Science **353**(6294), 62–67 (2016).
24. C. Bourassin-Bouchet, L. Barreau, V. Gruson, J.-F. Hergott, F. Quéré, P. Salières, and T. Ruchon, "Quantifying Decoherence in Attosecond Metrology," Phys. Rev. X **10**(3), 031048 (2020).
25. M. Kotur, D. Guénot, A. Jiménez-Galán, D. Kroon, E. W. Larsen, M. Louisy, S. Bengtsson, M. Miranda, J. Mauritsson, C. L. Arnold, S. E. Canton, M. Gisselbrecht, T. Carette, J. M. Dahlström, E. Lindroth, A. Maquet, L. Argenti, F. Martín, and A. L'Huillier, "Spectral phase measurement of a Fano resonance using tunable attosecond pulses," Nat. Commun. **7**(1), 10566 (2016).
26. C. Cirelli, C. Marante, S. Heuser, C. L. M. Petersson, A. J. Galán, L. Argenti, S. Zhong, D. Busto, M. Isinger, S. Nandi, S. Maclot, L. Rading, P. Johnsson, M. Gisselbrecht, M. Lucchini, L. Gallmann, J. M. Dahlström, E. Lindroth, A. L'Huillier, F. Martín, and U. Keller, "Anisotropic photoemission time delays close to a Fano resonance," Nat. Commun. **9**(1), 955 (2018).
27. H. Wei, T. Morishita, and C. D. Lin, "Critical evaluation of attosecond time delays retrieved from photoelectron streaking measurements," Phys. Rev. A **93**(5), 053412 (2016).
28. M. Wickenhauser, J. Burgdörfer, F. Krausz, and M. Drescher, "Time resolved fano resonances," Phys. Rev. Lett. **94**(2), 023002 (2005).
29. V. S. Yakovlev, J. Gagnon, N. Karpowicz, and F. Krausz, "Attosecond Streaking Enables the Measurement of Quantum Phase," Phys. Rev. Lett. **105**(7), 073001 (2010).
30. M. Lucchini, M. Brügmann, A. Ludwig, L. Gallmann, U. Keller, and T. Feurer, "Ptychographic reconstruction of attosecond pulses," Opt. Express **23**(23), 29502–29513 (2015).

Optics EXPRESS

31. W.-W. Yu, X. Zhao, H. Wei, S.-J. Wang, and C. D. Lin, "Method for spectral phase retrieval of single attosecond pulses utilizing the autocorrelation of photoelectron streaking spectra," Phys. Rev. A **99**(3), 033403 (2019).
32. Z. Zhu, J. White, Z. Chang, and S. Pang, "Attosecond pulse retrieval from noisy streaking traces with conditional variational generative network," Sci. Rep. **10**(1), 5782 (2020).
33. L. Pedrelli, P. D. Keathley, L. Cattaneo, F. X. Kärtner, and U. Keller, "Complete phase retrieval of photoelectron wavepackets," New J. Phys. **22**(5), 053028 (2020).
34. M. Kitzler, N. Milosevic, A. Scrinzi, F. Krausz, and T. Brabec, "Quantum theory of attosecond xuv pulse measurement by laser dressed photoionization," Phys. Rev. Lett. **88**(17), 173904 (2002).
35. Z. Chang, *Fundamentals of Attosecond Optics* (Chemical Rubber Company, 2016).
36. M. Lucchini, A. Ludwig, L. Kasmi, L. Gallmann, and U. Keller, "Semi-classical approach to compute rabbitt traces in multi-dimensional complex field distributions," Opt. Express **23**(7), 8867–8879 (2015).
37. Z. X. Zhao and C. D. Lin, "Theory of laser-assisted autoionization by attosecond light pulses," Phys. Rev. A **71**(6), 060702 (2005).
38. J. Bakos, "Ac stark effect and multiphoton processes in atoms," Phys. Rep. **31**(3), 209–235 (1977).
39. J. M. Dahlström, A. L'Huillier, and A. Maquet, "Introduction to attosecond delays in photoionization," J. Phys. B: At., Mol. Opt. Phys. **45**(18), 183001 (2012).
40. M. Ossiander, F. Siegrist, V. Shirvanyan, R. Pazourek, A. Sommer, T. Latka, A. Guggenmos, S. Nagele, J. Feist, J. Burgdörfer, R. Kienberger, and M. Schultze, "Attosecond correlation dynamics," Nat. Phys. **13**(3), 280–285 (2017).
41. M. Lucchini and M. Nisoli, "Refined Ptychographic Reconstruction of Attosecond Pulses," Appl. Sci. **8**(12), 2563 (2018).
42. X. Zhao, S.-J. Wang, W.-W. Yu, H. Wei, C. Wei, B. Wang, J. Chen, and C. D. Lin, "Metrology of Time-Domain Soft X-Ray Attosecond Pulses and Reevaluation of Pulse Durations of Three Recent Experiments," Phys. Rev. Appl. **13**(3), 034043 (2020).
43. D. Kane, "Recent progress toward real-time measurement of ultrashort laser pulses," IEEE J. Quantum Electron. **35**(4), 421–431 (1999).
44. J. Gagnon, E. Goulielmakis, and V. Yakovlev, "The accurate FROG characterization of attosecond pulses from streaking measurements," Appl. Phys. B **92**(1), 25–32 (2008).